Published in final edited form as:
Gastroenterology. 2005 April ; 128(4): 987–1001.

Distinct Temporal-Spatial Roles for Rho Kinase and Myosin Light Chain Kinase in Epithelial Purse-String Wound Closure

JOHN M. RUSSO[*], **PETER FLORIAN**[‡], **LE SHEN**[*], **W. VALLEN GRAHAM**[*], **MARIA S. TRETIAKOVA**[*], **ALFRED H. GITTER**[‡,§], **RANDALL J. MRSNY**[¶], and **JERROLD R. TURNER**[,*]

[*]*Department of Pathology, University of Chicago, Chicago, Illinois;* [‡]*Department of Clinical Physiology, Charité, Campus Benjamin Franklin, Berlin, Germany;* [§]*Department of Biophysics and Bioinformatics, Jena University of Applied Sciences, Jena, Germany; and* [¶]*Center for Drug Delivery, Welsh School of Pharmacy, Cardiff University, Cardiff, Wales*

Abstract

Background & Aims—Small epithelial wounds heal by purse-string contraction of an actomyosin ring that is regulated by myosin light chain (MLC) kinase (MLCK) and rho kinase (ROCK). These studies aimed to define the roles of these kinases in purse-string wound closure.

Methods—Oligocellular and single-cell wounds were created in intestinal epithelial monolayers. Fluorescence imaging and electrophysiologic data were collected during wound closure. Human biopsies were studied immunohistochemically.

Results—Live-cell imaging of enhanced green fluorescent protein-β-actin defined rapid actin ring assembly within 2 minutes after wounding. This progressed to a circumferential ring within 8 minutes that subsequently contracted and closed the wound. We therefore divided this process into 2 phases: ring assembly and wound contraction. Activated rho and ROCK localized to the wound edge during ring assembly. Consistent with a primary role in the assembly phase, ROCK inhibition prevented actin ring assembly and wound closure. ROCK inhibition after ring assembly was complete had no effect. Recruitment and activation of MLCK occurred after ring assembly was complete and coincided with ring contraction. MLCK inhibition slowed and then stopped contraction but did not prevent ring assembly. MLCK inhibition also delayed barrier function recovery. Studies of human colonic biopsy specimens suggest that purse-string wound closure also occurs in vivo, because MLC phosphorylation was enhanced surrounding oligocellular wounds.

Conclusions—These results suggest complementary roles for these kinases in purse-string closure of experimental and in vivo oligocellular epithelial wounds; rho and ROCK are critical for actin ring assembly, while the activity of MLCK drives contraction.

Abbreviations used in this paper

EGFP, enhanced green fluorescent protein; GST, glutathione S-transferase; MLC, myosin light chain; MLCK, myosin light chain kinase; ROCK, rho kinase

Address requests for reprints to: Jerrold R. Turner, MD, PhD, Department of Pathology, University of Chicago, 5841 South Maryland Avenue, MC 1089, Chicago, Illinois 60637. e-mail: jturner@bsd.uchicago.edu; fax: (773) 834–5251..

Supported by the Crohn's & Colitis Foundation of America (to J.R.T.), the National Institutes of Health (R01DK61931 to J.R.T. and T32DK07074 to support J.M.R.), the University of Chicago Digestive Disease Center (P30 DK42086), the University of Chicago Cancer Center (P30 CA14599), the Deutsche Forschungsgemeinschaft (GRK 276 to P.F. and A.H.G.), and Campus Benjamin Franklin Faculty funds (to P.F. and A.H.G.).

Dr Russo's current address is: Pediatric Gastroenterology and Nutrition, Ohio State University College of Medicine and Public Health, Columbus Children's Hospital, 700 Children's Drive, Columbus, Ohio 43205.

Like all epithelia, a primary function of the gastrointestinal epithelium is to provide a barrier to the noxious luminal milieu. This barrier must be maintained despite local epithelial damage that occurs regularly as a result of minor trauma, inflammation, and the physiologic shedding of apoptotic cells.[1–5] Thus, rapid and efficient closure of these wounds and restoration of barrier integrity are critical to normal function and prevention of disease.

Epithelial wound closure occurs by 2 distinct mechanisms: lamellipodia-dependent cell migration and coordinated purse-string contraction.[6,7] Larger wounds tend to heal by extension of lamellipodia from cells surrounding the wound followed by the migration of these cells to close the wound.[6,8] In contrast, small epithelial wounds, defined operationally as those <10 cells in diameter, close by purse-string contraction of a ring of actin filaments that form a continuous arc encircling the wound edge.[4,7,9] The force of this contraction is transmitted across cells via adherens junctions,[10] resulting in rapid restoration of barrier function.[9] This mechanism of wound closure is highly conserved developmentally and evolutionarily and has been demonstrated in embryonic chick wing buds[11] and closure of plasma membrane wounds within single *Xenopus* oocytes.[12]

A primary regulator of actomyosin contraction is phosphorylation of myosin light chain (MLC). Phosphorylation is typically accomplished by myosin light chain kinase (MLCK), which phosphorylates MLC at serine 19, thereby activating actomyosin contraction. Although recent studies have identified additional kinases that can phosphorylate MLC,[13–17] MLCK is the primary kinase responsible for MLC phosphorylation in intestinal epithelial cells.[18,19] Rho kinase (ROCK) can also regulate MLC phosphorylation, either by direct MLC phosphorylation[14] or by inhibition of MLC phosphatase leading to increased MLC phosphorylation.[20,21] Thus, although it is reasonable to hypothesize that MLC phosphorylation drives actomyosin contraction in epithelial purse-string wound closure, available data from disparate systems provide conflicting descriptions of the roles of rho, ROCK, MLCK, and MLC during this process.[4,9,12,14,22,23] We sought to define the recruitment, activation, and functional roles of these critical regulators in a well-characterized system of intestinal epithelial purse-string wound closure.

Using intestinal epithelial cells expressing an enhanced green fluorescent protein (EGFP)-β-actin fusion protein, we were able to characterize the reorganization of actin-containing structures during purse-string closure of oligocellular epithelial wounds. These real-time observations revealed a highly orchestrated, reproducible process that could be divided into 2 distinct phases. We then used immunostaining, highly specific pharmacologic inhibitors of MLCK and ROCK, and conductance scanning analyses to define the roles of these kinases in experimental purse-string wound closure and barrier restoration. Finally, we studied human biopsy specimens from a condition of increased epithelial cell turnover: active inflammatory bowel disease. The results suggest that ROCK and MLCK serve unique, complementary roles in oligocellular epithelial wound closure. These data therefore have direct implications for understanding the mechanisms of closure for physiologic wounds that occur in healthy individuals and pathologic wounds occurring in individuals with intestinal disease.

Materials and Methods

Wound Induction

Caco-2 BBe cells[24] expressing an EGFP/β-actin fusion protein were grown as monolayers on rat tail collagen-coated 35-mm cell culture dishes (Corning, Inc, Corning, NY). Dishes were placed on a 37°C heated stage in pH 7.4 HEPES-buffered Hanks' balanced salt solution (without bicarbonate) during wounding and subsequent imaging. Monolayers were treated with 10 μmol/L Y-27632 (Calbiochem, San Diego, CA) or 250 μmol/L PIK, an oligopeptide that is a specific membrane-permeant inhibitor of MLCK[25] before wounding. Wounds were created

manually using a 0.003-gauge tungsten wire (California Fine Wire, Grover Beach, CA) as described previously.[7]

Imaging

Wound closure in live cells was imaged using a 63X HCX Apo immersion objective and a DMLB epifluorescence microscope (Leica Microsystems, Wetzlar, Germany) equipped with an Endow GFP bandpass emission cube (Chroma Technology Corp, Brattleboro, VT) and Roper Coolsnap HQ camera controlled by MetaMorph 6 (Universal Imaging Corp, Downingtown, PA). Serial z-stack images, at 1-μm intervals, were obtained every 2 minutes after wounding. Fixed wounds were imaged after staining using a quad bandpass 88000 filter set (Chroma Technology Corp). Wound areas were determined using MetaMorph 6 after manually tracing the wound edge. Pixel intensities were determined with MetaMorph 6 using matched samples stained and imaged under identical conditions. For these analyses, pixel intensities along lines perpendicular to the wound edge were plotted. The peak actin intensity, corresponding to the developing or established actin ring, was used to align multiple lines and was arbitrarily designated zero. These analyses were performed for multiple wounds.

Monolayer Fixation and Staining

Wounds were fixed in 1% paraformaldehyde in phosphate-buffered saline at indicated times after wounding. Wound sites were labeled stereotactically to aid in identifying specific wounds after staining. After permeabilization with 0.1% Triton X-100 specific antibodies were applied. Activated rho was detected by incubation with a glutathione *S*-transferase (GST)-rhotekin rho binding domain fusion protein (Upstate Biotechnology, Lake Placid, NY) followed by incubation with polyclonal goat anti-GST (Amersham Biosciences, Piscataway, NJ) and then Alexa 594 donkey anti-goat immunoglobulin (Ig) G (Molecular Probes, Eugene, OR). Control experiments showed that substitution of GST/rhotekin with an irrelevant GST fusion protein did not label the wound edge but did nonspecifically label dead/damaged cells within the wound. ROCK was labeled using a mouse monoclonal anti–ROCK-I/ROK-β antibody (Becton Dickinson, Franklin Lakes, NJ) followed by Alexa-594 goat anti-mouse IgG (Molecular Probes). MLCK was detected using mouse monoclonal anti-MLCK clone K-36 (Sigma Chemical Co, St Louis, MO) followed by Alexa-594 goat anti-mouse IgG. Phosphorylated MLC was detected using affinity-purified polyclonal rabbit antisera, as described previously,[26] followed by Alexa-350 goat anti-rabbit antibody (Molecular Probes). In fixed preparations F-actin was stained using Alexa-488-phalloidin as described previously.[25] Activated MLCK was detected using biotinylated PIK and Alexa-594 streptavidin as described previously[25] and in Results. PIK labeling was assessed quantitatively using a fluorescent microplate reader (Synergy HT; Bio-Tek Instruments, Inc, Winooski, VT).

In Vitro Kinase Assays

Kinase assays were performed as described previously[25] using long MLCK[19,27] from Caco-2 cells and recombinant intestinal epithelial MLC. PIK or vehicle was added to reaction mixtures and the reaction initiated by the addition of γ-^{32}P–adenosine triphosphate (MP, Costa Mesa, CA) and 5 μmol/L recombinant MLC. MLC phosphorylation was determined by sodium dodecyl sulfate-polyacrylamide gel electrophoresis autoradiography of reaction mixtures.

Conductance Scanning

Monolayers were placed in a miniaturized Üssing chamber mounted on an upright light microscope. A sinusoidal electric current (100 μA/cm^2, 24 Hz) was clamped across the epithelium and the electric field generated in the mucosal bath measured with a mobile probe positioned at a constant distance of 25 μm above the apical surface. This spacing was readjusted at every measurement position as described previously.[28] The apparent conductivity G_A was

calculated from the scanning signal as previously described.[9] By scanning parallel to the epithelial surface, an area of at least 100 × 100 μm was chosen, where the spatial distribution of G_A was even. This value represented the conductivity of the intact epithelium (G^{intact}). Single-cell wounds were created using an additional glass microelectrode filled with 0.1 mol/L $CaCl_2$. The cell touched by the microelectrode flattened, and a current pulse (1.5 μA, 0.5 seconds) was applied.[9] These single-cell lesions created a local leak, with an increased G_A in close proximity. To record the time course of the leak current, the scan of G_A along the x-axis (directly above the lesion, x = 0, and x = 10, 20, 40, 70, and 100 μm apart) was repeated in intervals of 1–1.5 minutes. With these data, the conductance associated with a single leak (g^{leak}) was calculated by numerical integration of $G_A - G^{intact}$ as described previously.[9] The leak was determined between 2 and 16 minutes.

Human Colonic Biopsy Specimens

Formalin-fixed, paraffin-embedded human colonic biopsy specimens were selected from the archives of the Department of Pathology at the University of Chicago. The protocol for use of these specimens was approved by the institutional review board of the University of Chicago. Five-micrometer sections were stained by the immunoperoxidase technique using affinity-purified polyclonal rabbit anti-phosphorylated MLC as described previously.[26,29]

Results

Real-Time Analysis of Actin Dynamics During Purse-String Wound Closure

Previous work has shown that experimental oligocellular wounds within epithelial monolayers heal by a mechanism that involves the assembly and contraction of multicellular actin rings or purse-strings.[7] The process by which this occurs has not been defined. To define this process in detail, we analyzed purse-string wound closure in monolayers of Caco-2 human intestinal epithelial cells expressing EGFP-β-actin. This revealed a sequence of precisely orchestrated events that occurred with a high degree of reproducibility and was complete within 30–45 minutes (Figure 1 and Movie 1; see supplemental material online at www.gastrojournal.org). Closure occurred as a 2-phase process characterized by ring assembly followed by wound contraction. The first characteristic event was the assembly of actin filaments at the wound edge, consistent with local actin recruitment. This typically began within 2 minutes after wounding (Figure 1*A* at 2 minutes, arrow). At this time, EGFP fluorescence of dead cells within the wound was also apparent. Over the next several minutes, actin accumulation at the wound edge continued, ultimately forming a ring of actin that completely encircled the wound. By 8 minutes after wounding, a stable continuous ring had formed (Figure 1*A* at 8 minutes, arrow). Wound edge rounding, which indicated the development of tension within the ring, marked initiation of the second phase of wound closure, contraction. This coincided with initiation of quantitatively evident wound closure, which began at 6 – 8 minutes (Figure 1*B*). At this point, the wound rapidly decreased in area, resulting in stretching of cells surrounding the wound and a subtle flattening of some cells, causing portions of the monolayer to dip out of the plane of focus (Figure 1*A*).

Activated Rho Accumulates at the Wound Edge During Actin Filament Assembly

Rho and ROCK play an essential role in stress fiber assembly[30,31] and actomyosin contraction.[4,14,23] To define the roles of rho and ROCK in oligocellular epithelial purse-string wound closure, we began by defining the distributions of activated rho and ROCK during the wound closure process. We chose time points that corresponded to the initiation of the 2 phases of wound closure: ring assembly at 2 minutes after wounding and contraction at 8 minutes after wounding. To label activated rho morphologically, we adapted a well-characterized biochemical assay for detecting activated rho, binding of a GST fusion protein of the rho binding domain of rhotekin,[32] in a manner similar to an approach used to morphologically

detect activated cdc42.[33] As can be seen in cells away from the wound, activated rho was primarily localized to cell junctions before wounding. Within 2 minutes after wounding, when the ring assembly phase had begun, activated rho was concentrated at multiple sites along the wound edge, both in association with (Figure 2*A*, insets) and separate from (Figure 2*A*, arrows) sites of early actin accumulation. In some areas of the wound edge, actin and activated rho colocalization was apparent (Figure 2*A*, insets). Activated rho was also detected away from the developing actin ring (Figure 2*A*, top of field). An increase in cytoplasmic-activated rho was detected 8 minutes after wounding, when contraction began. However, this activated rho was primarily localized behind the actin ring (Figure 2*B*, inset, compare images of actin and activated rho in cells away from the wound). At 8 minutes, only small amounts of activated rho remained at the wound edge and did not colocalize with the actin ring. As seen in the live-cell imaging, damaged cells were commonly retained within the wound. These cells stained strongly (asterisk, Figure 2*B*) but nonspecifically, because they were also strongly labeled in wounds stained with an irrelevant GST fusion protein in place of the GST-rhotekin rho binding domain fusion protein and other antibodies (eg, Figures 3*B*, 5*A*, and 5*B*). Thus, activated rho is rapidly recruited to the wound edge during actin ring assembly but is not present at the wound edge as contraction begins.

ROCK Is Rapidly Recruited to the Wound

Rho is an upstream regulator of ROCK, which can regulate both actin polymerization and MLC phosphorylation.[14,20,34–41] We were interested in determining whether rho activation coincided with ROCK recruitment to the wound edge. ROCK was detected in punctate foci throughout the monolayer and was not localized to cell junctions or perijunctional actin before wounding. Within 2 minutes after wounding ROCK accumulated in discontinuous foci at and adjacent to the wound edge, both in association with actin (Figure 3*A*, insets) and separate from sites of actin assembly (Figure 3*A*, arrows). However, unlike activated rho, the distribution of ROCK remained punctate and decorated the developing actin ring in an irregular beaded pattern. Although this multifocal ROCK recruitment was easily appreciated on review of many wounds, it was subtle in any individual wound. Thus, we performed quantitative analysis of ROCK accumulation based on pixel intensity. The developing actin ring was used as a landmark to allow comparison of multiple areas of many wounds. As shown in the quantitative analysis (Figure 3*A*), a small peak of ROCK accumulation (Figure 3*A*, black arrow) was frequently detected ~1 μm in front (ie, closer to the center of the wound) of the developing actin ring. ROCK was also present in association with the actin ring itself.

In contrast to the appearance 2 minutes after wounding, by 8 minutes, when contraction began, ROCK was easily detectable within the cytoplasm away from the wound edge and in association with the actin ring but was no longer present at the wound edge (Figure 3*B*, insets). Quantitative analysis of pixel intensity showed increased actin accumulation at the wound edge (compare the area under the curve for actin with that in Figure 3*A*). However, in contrast to the earlier time point, ROCK was not detected ahead of the actin ring (Figure 3*B*, black arrow). Thus, the morphologic and quantitative analyses show that ROCK was recruited to the wound edge during the ring assembly phase of wound closure. At later times, an association between ROCK and the actin ring persisted but local recruitment of ROCK to the leading edge of the wound, just ahead of the actin ring, was not detected.

ROCK Activity Is Required for Actin Ring Assembly

Because activated rho and ROCK are recruited to the wound edge in the early stages of wound closure, but not in the later stages, the localization data suggest that the primary roles of activated rho and ROCK may be during the ring assembly phase. To directly evaluate the role of ROCK in epithelial purse-string wound closure, we evaluated wound closure in monolayers treated with the specific ROCK inhibitor Y-27632.[42] Small foci of actin recruitment were seen

within the first minutes after injury (Figure 4 and Movie 2; see supplemental material online at www.gastrojournal.org). However, these foci were transient when ROCK was inhibited (Figure 4*A*, 8 minutes and 12 minutes, arrows). Analysis of 3-dimensional reconstructions collected during wound closure confirmed that neither an intact actin ring nor stable arcs of actin were present when ROCK was inhibited. Wound edges did not round, and there was no evidence of a contraction phase. Filopodial extensions, which were never detected in control wounds, were seen when ROCK was inhibited (Figure 4*A*, 20 minutes, arrow). However, these filopodia were transient and did not lead to any meaningful wound closure. Some movement of cells surrounding the wound did occur after wounding (Figure 4*A*, 32 minutes), but meaningful coordinated movement of these cells was not present when ROCK was inhibited. As in control monolayers, dead cells were often prominent within wounds in monolayers treated with Y-27632 (Figure 4*A*, asterisks). However, these often remained visible at late time points to the extent that, on casual examination, it might appear that the wound closed. Despite this retention of dead cells, careful examination of 3-dimensional reconstructions of the time-lapse images and quantitative analysis of wound area (Figure 4*B*) showed that Y-27632 prevented coordinated purse-string contraction and wound closure for at least 2 hours after wounding.

These data suggest that ROCK may direct actin ring assembly during the early stage of purse-string wound closure. However, it is possible that ROCK might also regulate contraction via phosphorylation of MLC or MYPT1.[14,20,21] To determine if ROCK is necessary for wound contraction, wounds were treated with Y-27632 after ring assembly was nearly complete (ie, 6 minutes after wounding). In these wounds, the wound area decreased with kinetics nearly identical to control wounds (Figure 4*B*) and the morphology of wound closure was similar to that of control wounds (Figure 4*C*). Together with the early recruitment of activated rho and ROCK to the wound edge, these data suggest that the primary roles of rho and ROCK in purse-string wound closure occur early and are to direct the assembly and maintenance of actin filaments at the wound edge. The data also suggest that ROCK activity is not necessary for actomyosin ring contraction.

Recruitment and Activation of MLCK Coincides With MLC Phosphorylation and the Initiation of Wound Contraction

A principal determinant of actomyosin contraction is the status of MLC phosphorylation. We have previously shown that, in Caco-2 intestinal epithelial cells, MLCK is the primary kinase that phosphorylates MLC.[18,19] While MLC phosphorylation in smooth muscle can also be regulated by ROCK-dependent processes,[14,20,43] the data above suggest that ROCK is not necessary for the contraction phase of purse-string wound closure. Thus, we evaluated the contribution of MLCK to this process. Within 2 minutes after wounding, at which time ring assembly had begun and accumulation of activated rho and ROCK was maximal, MLCK and phosphorylated MLC were only focally present at the wound edge (Figure 5*A*). However, 6 minutes later, when contraction began, phosphorylated MLC was present in a nearly circumferential ring at the wound edge that colocalized with the contracting actomyosin ring (Figure 5*B*, insets). MLCK decorated the actomyosin ring in a punctate pattern. This spatiotemporal correlation of MLCK recruitment, MLC phosphorylation, and actomyosin ring contraction suggests that MLCK-dependent MLC phosphorylation drives the contractile phase of wound closure.

To determine if MLCK was activated at this site, we developed a morphologic probe specific for activated MLCK. Design of this probe is based on the fact that the peptide MLCK inhibitor PIK[25] binds with high affinity to the exposed catalytic domain when MLCK is in the active configuration (Figure 6*A*). Thus, we hypothesized that when MLCK is cross-linked in a static configuration by aldehyde fixation, PIK can bind to active, but not inactive, MLCK (Figure

6*A*). We used a biotinylated PIK peptide to allow localization of PIK binding using fluorescent streptavidin conjugates. Consistent with this, we have shown that PIK preferentially binds to a site enriched in MLC phosphorylated by MLCK, the perijunctional actomyosin ring, in intact epithelial monolayers (Figure 6*B*).[25,26] We also found that, in migrating Caco-2 cells, PIK was highly concentrated within lamellipodia, consistent with the known site of MLCK activation in migrating cells.[44] Finally, to quantitatively evaluate PIK binding to the MLCK catalytic domain, we used Caco-2 cells that express the catalytic subunit of MLCK under the control of an inducible expression system.[45] Graduated induction of gene expression resulted in increased PIK labeling that correlated closely with the extent of MLCK catalytic subunit expression (Figure 6*C*; $r^2 = 0.98$). Thus, based on independent qualitative morphologic and quantitative analyses, biotinylated PIK labeling is an indicator of MLCK activation in fixed cells.

We used biotinylated PIK binding to ask if MLCK is activated at the wound edge during contraction. Consistent with the absence of immunohistochemically detectable MLCK at the wound edge within 2 minutes after wounding (eg, Figure 5*A*), activated MLCK was not detected at the wound edge during ring assembly (Figure 6*D*). In contrast, when contraction began and MLCK was present at the wound edge, activated MLCK was detected within discrete foci at the wound edge (Figure 6*E*). Notably, this activity was not continuous along the wound edge. One possible explanation for this distribution is that MLCK activity may not be uniformly present throughout the actomyosin ring at individual times. Although the data do not prove this point, this hypothesis is consistent with the observation that many wounds form an elliptical shape during closure, indicating nonuniform development of tension throughout the actin ring. Alternatively, this could also represent incomplete detection of activated MLCK by PIK, although PIK binding to the perijunctional actin in intact monolayers was uniform and continuous (Figure 6*B*). Regardless, the observations that MLCK, activated MLCK, and phosphorylated MLC all accumulate at the wound edge as contraction is initiated suggest that recruitment and activation of MLCK with subsequent MLC phosphorylation may contribute to contraction during purse-string wound closure.

MLCK Activity Is Required for the Contraction Phase of Wound Closure

The morphologic analyses above suggest that MLCK activity may be essential to the contraction phase of purse-string wound closure. To evaluate this functionally, we used PIK as a specific inhibitor of MLCK.[25,46] As shown previously,[25] this linear oligopeptide[46] is a potent and specific inhibitor of intestinal epithelial MLCK (Figure 7*C*). By virtue of its sequence homology to protein transduction domains,[47,48] PIK enters the cytoplasm and inhibits intracellular MLCK.[25]

In contrast to ROCK inhibition, inhibition of MLCK did not prevent actomyosin ring assembly (Figure 7*A* and Movie 3; see supplemental material online at www.gastrojournal.org). Actin polymerization occurred similarly to that in untreated monolayers (arrows at 2 and 12 minutes), and wound area was comparable to that of control wounds during the first 6 minutes after wounding (Figure 7*B*). Wound edges also began to round, indicative of the initial development of tension within the actin ring. However, by 8 minutes after wounding, when contraction began to accelerate in control wounds, MLCK inhibition caused contraction to stall (Figure 7*B*). At later times, the actin ring began to fragment (arrow at 56 minutes), wound edges became irregular, rather than rounded, and the wound returned to its original area (Figure 7*A*). Thus, although ring assembly occurred, contraction was blocked when MLCK activity was inhibited. Thus, these data suggest that although MLCK activity is not necessary for ring assembly, it is required for contraction during purse-string wound closure.

MLCK Inhibition Delays Restoration of Barrier Function During Purse-String Closure of Single-Cell Wounds

Restoration of barrier function is a critical end point of wound closure. We therefore analyzed restoration of barrier function in single cell wounds, which have been shown to close by purse-string actomyosin contraction.[9] Individual cells in an intact monolayer were destroyed with a current pulse delivered from a microelectrode. Conductance scanning[28] showed that this resulted in a local current leak (g^{leak}), whose magnitude decreased exponentially as the barrier was restored (Figure 8). From 2 minutes postlesion to 8 minutes postlesion, g^{leak} decreased by 53% in control monolayers. With increasing time of repair, g^{leak} decreased toward zero and the repaired epithelium assumed a tightness similar to that of undisturbed epithelium. Previous studies have shown that inhibition of ROCK with Y-27632 does not change the rate or extent of barrier recovery.[9] In contrast, inhibition of MLCK with PIK resulted in a marked slowing of repair (Figure 8). Between 2 minutes and 8 minutes after creating the lesion, g^{leak} decreased by only 36%. This corresponds to a 74% increase in the time constant for recovery, with significantly higher g^{leak} values at 8 and 16 minutes after wounding relative to control wounds ($P < .05$). Therefore, like larger wounds, purse-string closure of single-cell wounds requires MLCK activity.

MLC Phosphorylation Accompanies In Vivo Closure of Oligocellular Epithelial Wounds

The data above show that MLCK-mediated MLC phosphorylation is critical to epithelial purse-string wound closure in these reductionist experimental models. To determine whether these observations are relevant to closure of small wounds occurring in vivo, MLC phosphorylation was assessed in small wounds within rapidly fixed biopsy specimens of human colonic mucosa. Because these wounds are short lived and believed to be relatively infrequent in non-diseased mucosa, we studied mucosa involved by active inflammatory bowel disease, where epithelial injury occurs more frequently. MLC phosphorylation was markedly enhanced at the edges of oligocellular wounds in a manner similar to that seen in the experimental wounds (Figure 9, compare with Figure 5*B*). Because each biopsy represents a single time point, analysis of the overall process depends on its reconstruction from multiple individual wounds. Using the experimental wounds as a conceptual framework, we were able to assemble a series of oligocellular wounds suggesting that a similar MLCK-dependent process heals oligocellular wounds in vivo in human intestinal mucosa.

Discussion

The epithelial barrier is critical to homeostasis. Because most epithelia are in continuous contact with a foreign and potentially harmful environment, a rapid and efficient mechanism to correct damage to this barrier must be in place. For small wounds, this takes the form of purse-string contraction[4,7,9] rather than the slower lamellipodia-dependent cell migration typical of larger wounds.[6,49] This purse-string mechanism depends on the assembly of a circumferential contractile actomyosin ring surrounding the wound[7] and is used in a broad range of situations, including embryonic wound healing,[11] apoptotic cell extrusion,[4] and closure of plasma membrane wounds.[12] Many of these processes occur in both healthy individuals and patients with intestinal disease. Thus, understanding the coordinated process of purse-string wound closure, which likely occurs far more frequently than migration-dependent closure of larger wounds, also has therapeutic implications, as new therapies that inhibit ROCK or MLCK have been proposed for a variety of intestinal and extraintestinal diseases, including cancer metastasis, acute lung injury, and inflammatory bowel disease.[25, 50–53] Therefore, definition of these mechanisms may allow early identification and intervention to minimize intestinal toxicity of these agents.

Because phosphorylation of the MLC is a primary regulator of actomyosin contraction, we posited that contraction of this actomyosin ring might depend on MLC phosphorylation. However, available data from disparate systems provide conflicting descriptions of the roles of rho, ROCK, MLCK, and MLC during purse-string actomyosin contraction.[4,9,12,14,20,22,23] We sought to define the recruitment and activation patterns of these critical regulators in well-characterized in vitro systems of epithelial purse-string wound closure and in human biopsy specimens. We used live-cell imaging of EGFP-β-actin–expressing intestinal epithelial cells to follow actin dynamics in living cells during wound closure. This allowed us to define epithelial purse-string wound closure as a stepwise and precisely regulated process. Wound closure was reproducible and rapid, with the first recognizable event being actin concentration at the wound edge. This began within 2 minutes and was complete, with a continuous band of actin surrounding the wound edge, within 8 minutes after wounding. Initiation of this ring assembly phase coincided with recruitment of activated rho and its downstream effector ROCK to the wound edge. At the earliest time points activated rho and ROCK were present both in association with and separate from the initial sites of actin ring assembly. Thus, together with the observation that ROCK inhibition prevented ring assembly, these data suggest that ROCK may actually trigger ring assembly. This hypothesis is consistent with observations in 2 related models, healing of incisional wounds in the embryonic chick wing bud and puncture wounds in *Xenopus* oocytes, showing that rho is required for actin ring assembly.[12,23] Rho activity is also required for the assembly of actin bundles at wound edges in larger wounds, although neither rho activity nor formation of the bundles themselves is necessary for closure of these large wounds by lamellipodia-dependent cell migration.[8] Thus, consistent with the roles of rho and rho family members in stress fiber assembly and actin polymerization in systems as diverse as *Acanthamoeba* and fibroblasts,[30,31,54] these data suggest that the roles of rho and ROCK in purse-string wound closure are to direct assembly of the actin ring. Because ROCK inhibition did not prevent contraction, our data also suggest that ROCK activity is not necessary for the second phase of purse-string wound closure. Our observation that transient filopodia were seen when ROCK was inhibited, but never in control wounds, suggest that, in the absence of ring assembly, alternative mechanisms of wound closure can be activated. This hypothesis is consistent with a recent study showing that small wounds in *Drosophila* embryos, which normally heal by purse-string contraction, close using filopodial extensions in rho knockout flies.[55]

The absolute requirement for ROCK in purse-string closure of oligocellular epithelial wounds is at odds with work showing that barrier function recovers normally following the creation of single-cell wounds in intestinal epithelial monolayers treated with ROCK inhibitors[9] but is consistent with studies in renal epithelia showing that ROCK inhibition blocks apoptotic cell extrusion, a process that also appears to occur via purse-string actomyosin contraction.[4] While available data do not explain the differences between these disparate results in these unique experimental systems, it is important to note that the diameter of single-cell wounds induced with a current pulse (5–7 μm) is far less than the 20–40 μm diameter of the still quite small oligocellular wounds made by mechanical disruption. Thus, one possibility is that preexisting perijunctional actin rings that encircle each cell in an intact monolayer are sufficient to allow progression to the MLCK-dependent contraction phase in single-cell wounds, while ROCK-directed ring assembly is necessary in larger oligocellular wounds.

In normal wound healing, actin ring assembly is followed by contraction. We have shown that contraction begins within 8 minutes after wounding, as ring assembly is completed, and can initially be identified as wound edge rounding, signaling the development of tension within the actin ring. This process continues until wound closure is complete. The critical role for MLCK in wound closure is emphasized by the coincidence of the recruitment and activation of MLCK with MLC phosphorylation and the initiation of wound closure. The effects of the specific peptide inhibitor of MLCK, PIK, also support the essential role of MLCK in late phases

of wound closure. Thus, the data suggest that MLCK, and not ROCK, mediates the phosphorylation of MLC that is necessary for purse-string contraction.

The use of the peptide inhibitor of MLCK, PIK, directed against the substrate-binding site is a significant advance over previous studies using other inhibitors that target the adenosine triphosphate–binding site of MLCK. For example, the most commonly used MLCK inhibitor, ML-7, inhibits adenosine 3′,5′-cyclic monophosphate–dependent protein kinase with a K_i close to that for MLCK, while PIK does not inhibit adenosine 3′,5′-cyclic monophosphate–dependent protein kinase appreciably at any concentration.[46] Moreover, the observation that biotinylated PIK can be used as a specific probe for activated MLCK in fixed cells will likely make this an important tool in future work.

While these studies are not possible in intact tissues, we have asked whether components of this wound closure pathway can be identified in vivo. We analyzed oligocellular wounds in colonic mucosa from patients with active inflammatory bowel disease. MLC phosphorylation was markedly enhanced at the edges of oligocellular wounds in a pattern strikingly similar to that observed in the in vitro model. Thus, these data suggest that this mechanism of wound closure is active in vivo as well as in vitro.

Together the data suggest a model of epithelial purse-string wound closure where the rho-ROCK and MLCK pathways of actomyosin regulation serve spatially and temporally distinct functions (Figure 10). In this model, rho is rapidly recruited to and activated at the wound edge where it activates ROCK. ROCK then directs local actin polymerization, resulting in the coordinated assembly of a circumferential actin ring at the wound edge. MLCK recruitment and activation and the resulting MLC phosphorylation then drive actomyosin contraction. This culminates with restoration of epithelial barrier function. Thus, we have shown epithelial purse-string wound closure to be a precisely orchestrated process that can be separated into 2 distinct phases regulated by separate kinases: ROCK and MLCK.

Acknowledgements

The authors thank Drs Michael Fromm, Mark Musch, Daniel Clayburgh, and Stephen Meredith for helpful comments; Edwina Witkowski, Yingmin Wang, Helene Auer, Can Gong, and Sara Palkon for expert technical assistance; M. Wozniak and P. Keely for advice regarding staining of activated rho; and Vytautas Bindokas for inspired cover art assistance.

Appendix Supplementary Data

Supplementary data associated with this article can be found, in the online version, at doi: 10.1053/j.gastro.2005.01.004

References

1. Madara JL. Maintenance of the macromolecular barrier at cell extrusion sites in intestinal epithelium: physiological rearrangement of tight junctions. J Membr Biol 1990;116:177–184. [PubMed: 2380981]
2. Abreu MT, Palladino AA, Arnold ET, Kwon RS, McRoberts JA. Modulation of barrier function during Fas-mediated apoptosis in human intestinal epithelial cells. Gastroenterology 2000;119:1524–1536. [PubMed: 11113074]
3. Gitter AH, Bendfeldt K, Schulzke JD, Fromm M. Leaks in the epithelial barrier caused by spontaneous and TNF-alpha-induced single-cell apoptosis. FASEB J 2000;14:1749–1753. [PubMed: 10973924]
4. Rosenblatt J, Raff MC, Cramer LP. An epithelial cell destined for apoptosis signals its neighbors to extrude it by an actin- and myosin-dependent mechanism. Curr Biol 2001;11:1847–1857. [PubMed: 11728307]

5. Bruewer M, Luegering A, Kucharzik T, Parkos CA, Madara JL, Hopkins AM, Nusrat A. Proinflammatory cytokines disrupt epithelial barrier function by apoptosis-independent mechanisms. J Immunol 2003;171:6164–6172. [PubMed: 14634132]
6. Nusrat A, Delp C, Madara JL. Intestinal epithelial restitution. Characterization of a cell culture model and mapping of cytoskeletal elements in migrating cells. J Clin Invest 1992;89:1501–1511. [PubMed: 1569187]
7. Bement WM, Forscher P, Mooseker MS. A novel cytoskeletal structure involved in purse string wound closure and cell polarity maintenance. J Cell Biol 1993;121:565–578. [PubMed: 8486737]
8. Fenteany G, Janmey PA, Stossel TP. Signaling pathways and cell mechanics involved in wound closure by epithelial cell sheets. Curr Biol 2000;10:831–838. [PubMed: 10899000]
9. Florian P, Schoneberg T, Schulzke JD, Fromm M, Gitter AH. Single-cell epithelial defects close rapidly by an actinomyosin purse string mechanism with functional tight junctions. J Physiol 2002;545:485–499. [PubMed: 12456828]
10. Danjo Y, Gipson IK. Actin 'purse string' filaments are anchored by E-cadherin-mediated adherens junctions at the leading edge of the epithelial wound, providing coordinated cell movement. J Cell Sci 1998;111:3323–3332. [PubMed: 9788874]
11. Martin P, Lewis J. Actin cables and epidermal movement in embryonic wound healing. Nature 1992;360:179–183. [PubMed: 1436096]
12. Bement WM, Mandato CA, Kirsch MN. Wound-induced assembly and closure of an actomyosin purse string in *Xenopus* oocytes. Curr Biol 1999;9:579–587. [PubMed: 10359696]
13. Chew TL, Masaracchia RA, Goeckeler ZM, Wysolmerski RB. Phosphorylation of non-muscle myosin II regulatory light chain by p21-activated kinase (gamma-PAK). J Muscle Res Cell Motil 1998;19:839–854. [PubMed: 10047984]
14. Amano M, Ito M, Kimura K, Fukata Y, Chihara K, Nakano T, Matsuura Y, Kaibuchi K. Phosphorylation and activation of myosin by Rho-associated kinase (Rho-kinase). J Biol Chem 1996;271:20246–20249. [PubMed: 8702756]
15. Jin Y, Blue EK, Dixon S, Hou L, Wysolmerski RB, Gallagher PJ. Identification of a new form of death-associated protein kinase that promotes cell survival. J Biol Chem 2001;276:39667–39678. [PubMed: 11485996]
16. Komatsu S, Ikebe M. ZIP kinase is responsible for the phosphorylation of myosin II and necessary for cell motility in mammalian fibroblasts. J Cell Biol 2004;165:243–254. [PubMed: 15096528]
17. Yamashiro S, Totsukawa G, Yamakita Y, Sasaki Y, Madaule P, Ishizaki T, Narumiya S, Matsumura F. Citron kinase, a Rho-dependent kinase, induces di-phosphorylation of regulatory light chain of myosin II. Mol Biol Cell 2003;14:1745–1756. [PubMed: 12802051]
18. Turner JR, Angle JM, Black ED, Joyal JL, Sacks DB, Madara JL. Protein kinase C-dependent regulation of transepithelial resistance: the roles of myosin light chain and myosin light chain kinase. Am J Physiol 1999;277:C554–C562. [PubMed: 10484342]
19. Clayburgh DR, Rosen S, Witkowski ED, Wang F, Blair S, Dudek S, Garcia JGN, Alverdy JC, Turner JR. A differentiation-dependent splice variant of myosin light chain kinase, MLCK1, regulates epithelial tight junction permeability. J Biol Chem 2004;279:55506–55513. [PubMed: 15507455]
20. Kimura K, Ito M, Amano M, Chihara K, Fukata Y, Nakafuku M, Yamamori B, Feng J, Nakano T, Okawa K, Iwamatsu A, Kaibuchi K. Regulation of myosin phosphatase by Rho and Rho-associated kinase (Rho-kinase). Science 1996;273:245–248. [PubMed: 8662509]
21. Ito M, Nakano T, Erdodi F, Hartshorne DJ. Myosin phosphatase: structure, regulation and function. Mol Cell Biochem 2004;259:197–209. [PubMed: 15124925]
22. Matsumura F, Ono S, Yamakita Y, Totsukawa G, Yamashiro S. Specific localization of serine 19 phosphorylated myosin II during cell locomotion and mitosis of cultured cells. J Cell Biol 1998;140:119–129. [PubMed: 9425160]
23. Brock J, Midwinter K, Lewis J, Martin P. Healing of incisional wounds in the embryonic chick wing bud: characterization of the actin purse-string and demonstration of a requirement for Rho activation. J Cell Biol 1996;135:1097–1107. [PubMed: 8922389]
24. Peterson MD, Mooseker MS. Characterization of the enterocyte-like brush border cytoskeleton of the C2BBe clones of the human intestinal cell line, Caco-2. J Cell Sci 1992;102:581–600. [PubMed: 1506435]

25. Zolotarevsky Y, Hecht G, Koutsouris A, Gonzalez DE, Quan C, Tom J, Mrsny RJ, Turner JR. A membrane-permeant peptide that inhibits MLC kinase restores barrier function in in vitro models of intestinal disease. Gastroenterology 2002;123:163–172. [PubMed: 12105845]
26. Berglund JJ, Riegler M, Zolotarevsky Y, Wenzl E, Turner JR. Regulation of human jejunal transmucosal resistance and MLC phosphorylation by Na^+-glucose cotransport. Am J Physiol Gastrointest Liver Physiol 2001;281:G1487–G1493. [PubMed: 11705754]
27. Stull JT. Myosin minireview series. J Biol Chem 1996;271:15849. [PubMed: 8663555]
28. Gitter AH, Bertog M, Schulzke J, Fromm M. Measurement of paracellular epithelial conductivity by conductance scanning. Pflugers Arch 1997;434:830–840. [PubMed: 9306019]
29. Turner JR, Torres CM, Wang HH, Shahsafaei A, Richards WG, Sugarbaker D, Odze RD. Preoperative chemoradiotherapy alters the expression and prognostic significance of adhesion molecules in Barrett's-associated adenocarcinoma. Hum Pathol 2000;31:347–353. [PubMed: 10746678]
30. Ridley AJ, Hall A. The small GTP-binding protein rho regulates the assembly of focal adhesions and actin stress fibers in response to growth factors. Cell 1992;70:389–399. [PubMed: 1643657]
31. Nobes CD, Hall A. Rho, rac, and cdc42 GTPases regulate the assembly of multimolecular focal complexes associated with actin stress fibers, lamellipodia, and filopodia. Cell 1995;81:53–62. [PubMed: 7536630]
32. Ren XD, Kiosses WB, Schwartz MA. Regulation of the small GTP-binding protein Rho by cell adhesion and the cytoskeleton. EMBO J 1999;18:578–585. [PubMed: 9927417]
33. Cannon JL, Labno CM, Bosco G, Seth A, McGavin MH, Siminovitch KA, Rosen MK, Burkhardt JK. Wasp recruitment to the T cell:APC contact site occurs independently of Cdc42 activation. Immunity 2001;15:249–259. [PubMed: 11520460]
34. Chihara K, Amano M, Nakamura N, Yano T, Shibata M, Tokui T, Ichikawa H, Ikebe R, Ikebe M, Kaibuchi K. Cytoskeletal rearrangements and transcriptional activation of c-fos serum response element by Rho-kinase. J Biol Chem 1997;272:25121–25127. [PubMed: 9312122]
35. Katoh K, Kano Y, Amano M, Kaibuchi K, Fujiwara K. Stress fiber organization regulated by MLCK and Rho-kinase in cultured human fibroblasts. Am J Physiol Cell Physiol 2001;280:C1669–C1679. [PubMed: 11350763]
36. Katoh K, Kano Y, Amano M, Onishi H, Kaibuchi K, Fujiwara K. Rho-kinase–mediated contraction of isolated stress fibers. J Cell Biol 2001;153:569–584. [PubMed: 11331307]
37. Vasiliev JM, Omelchenko T, Gelfand IM, Feder HH, Bonder EM. Rho overexpression leads to mitosis-associated detachment of cells from epithelial sheets: a link to the mechanism of cancer dissemination. Proc Natl Acad Sci U S A 2004;101:12526–12530. [PubMed: 15304643]
38. Anderson S, DiCesare L, Tan I, Leung T, SundarRaj N. Rho-mediated assembly of stress fibers is differentially regulated in corneal fibroblasts and myofibroblasts. Exp Cell Res 2004;298:574–583. [PubMed: 15265703]
39. Kawabata S, Usukura J, Morone N, Ito M, Iwamatsu A, Kaibuchi K, Amano M. Interaction of Rho-kinase with myosin II at stress fibres. Genes Cells 2004;9:653–660. [PubMed: 15265008]
40. Higashida C, Miyoshi T, Fujita A, Oceguera-Yanez F, Monypenny J, Andou Y, Narumiya S, Watanabe N. Actin polymerization-driven molecular movement of mDia1 in living cells. Science 2004;303:2007–2010. [PubMed: 15044801]
41. Totsukawa G, Wu Y, Sasaki Y, Hartshorne DJ, Yamakita Y, Yamashiro S, Matsumura F. Distinct roles of MLCK and ROCK in the regulation of membrane protrusions and focal adhesion dynamics during cell migration of fibroblasts. J Cell Biol 2004;164:427–439. [PubMed: 14757754]
42. Uehata M, Ishizaki T, Satoh H, Ono T, Kawahara T, Morishita T, Tamakawa H, Yamagami K, Inui J, Maekawa M, Narumiya S. Calcium sensitization of smooth muscle mediated by a Rho-associated protein kinase in hypertension. Nature 1997;389:990–994. [PubMed: 9353125]
43. Kawano Y, Fukata Y, Oshiro N, Amano M, Nakamura T, Ito M, Matsumura F, Inagaki M, Kaibuchi K. Phosphorylation of myosin-binding subunit (MBS) of myosin phosphatase by Rho-kinase in vivo. J Cell Biol 1999;147:1023–1038. [PubMed: 10579722]
44. Chew TL, Wolf WA, Gallagher PJ, Matsumura F, Chisholm RL. A fluorescent resonant energy transfer-based biosensor reveals transient and regional myosin light chain kinase activation in lamella and cleavage furrows. J Cell Biol 2002;156:543–553. [PubMed: 11815633]

45. Turner JR, Guerriero V Jr, Black ED, Haelewyn K. Regulated expression of the myosin light chain kinase catalytic domain increases paracellular permeability and alters tight junction structure (abstr). Gastroenterology 2000;118:A432.

46. Lukas TJ, Mirzoeva S, Slomczynska U, Watterson DM. Identification of novel classes of protein kinase inhibitors using combinatorial peptide chemistry based on functional genomics knowledge. J Med Chem 1999;42:910–919. [PubMed: 10072688]

47. Schwarze SR, Ho A, Vocero-Akbani A, Dowdy SF. In vivo protein transduction: delivery of a biologically active protein into the mouse. Science 1999;285:1569–1572. [PubMed: 10477521]

48. Wadia JS, Stan RV, Dowdy SF. Transducible TAT-HA fusogenic peptide enhances escape of TAT-fusion proteins after lipid raft macropinocytosis. Nat Med 2004;10:310–315. [PubMed: 14770178]

49. Basson MD, Modlin IM, Madri JA. Human enterocyte (Caco-2) migration is modulated in vitro by extracellular matrix composition and epidermal growth factor. J Clin Invest 1992;90:15–23. [PubMed: 1634605]

50. Takamura M, Sakamoto M, Genda T, Ichida T, Asakura H, Hirohashi S. Inhibition of intrahepatic metastasis of human hepatocellular carcinoma by Rho-associated protein kinase inhibitor Y-27632. Hepatology 2001;33:577–581. [PubMed: 11230737]

51. Clayburgh DR, Shen L, Turner JR. A porous defense: the leaky epithelial barrier in intestinal disease. Lab Invest 2004;84:282–291. [PubMed: 14767487]

52. Wainwright MS, Rossi J, Schavocky J, Crawford S, Steinhorn D, Velentza AV, Zasadzki M, Shirinsky V, Jia Y, Haiech J, Van Eldik LJ, Watterson DM. Protein kinase involved in lung injury susceptibility: evidence from enzyme isoform genetic knockout and in vivo inhibitor treatment. Proc Natl Acad Sci U S A 2003;100:6233–6238. [PubMed: 12730364]

53. Dull RO, Garcia JG. Leukocyte-induced microvascular permeability: how contractile tweaks lead to leaks. Circ Res 2002;90:1143–1144. [PubMed: 12065313]

54. Mullins RD, Pollard TD. Rho-family GTPases require the Arp2/3 complex to stimulate actin polymerization in *Acanthamoeba* extracts. Curr Biol 1999;9:405–415. [PubMed: 10226024]

55. Wood W, Jacinto A, Grose R, Woolner S, Gale J, Wilson C, Martin P. Wound healing recapitulates morphogenesis in *Drosophila* embryos. Nat Cell Biol 2002;4:907–912. [PubMed: 12402048]

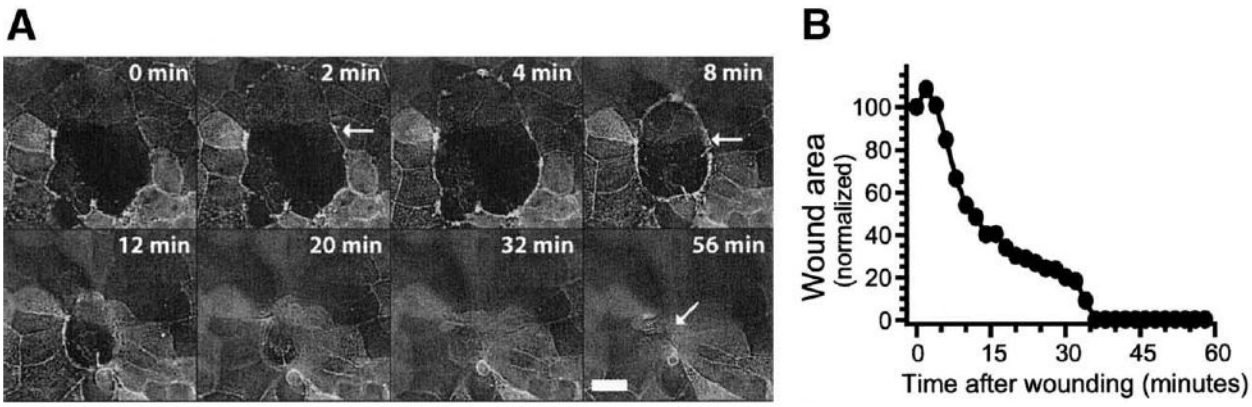

Figure 1.

(*A*) Real-time analysis of actin dynamics during purse-string wound closure in Caco-2 cells (also see Movie 1; see supplemental material online at www.gastrojournal.org). Closure of oligocellular epithelial wounds was analyzed in Caco-2 cells stably expressing EGFP-β-actin. Within 2 minutes after wounding, actin polymerization occurred at the wound edge (*arrow*). Residual EGFP fluorescence of dead cells retained within the wound is apparent at time points up to 8 minutes (note top of wound). By 8 minutes, a continuous ring of actin (*arrow*) was present and the wound rounded, indicating the development of circumferential tension. This was followed by contraction of the actomyosin ring as the wound closed. Most activity occurred within the first 32 minutes and wound closure was complete before 56 minutes (*arrow*). The wound-healing process was associated with stretching and flattening of some cells, resulting in a gradual shift of some areas out of the plane of focus. *Bar* = 20 μm. (*B*) Wound closure occurs rapidly following an initial lag. Wound area was measured at intervals throughout the healing process and normalized to the initial wound area. Wound area began to decrease rapidly 6–8 minutes after injury. Wound closure was complete within 30–45 minutes. Data are representative of more than 20 similar experiments.

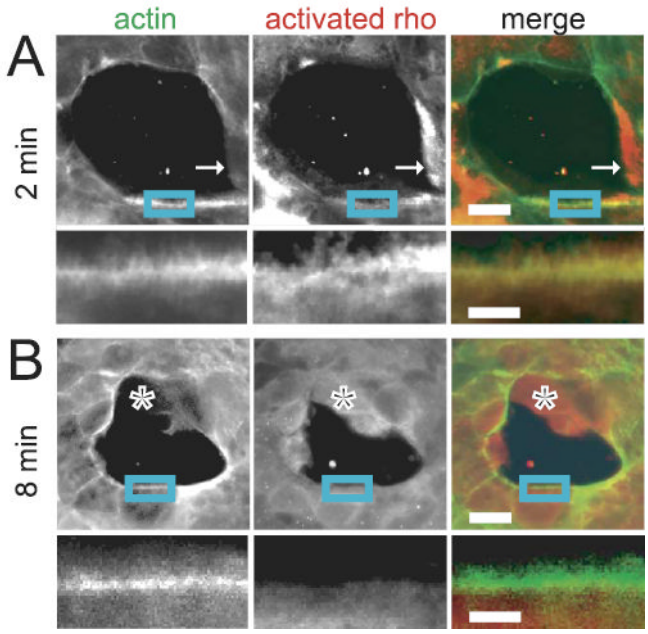

Figure 2.

(*A*) Activated rho is present at the wound edge 2 minutes after wounding. Staining for activated rho (*red* in merged image) revealed its presence in multiple foci along the wound edge within 2 minutes of wounding, both in areas with (*insets*) and without (*arrows*) early actin accumulation (*green* in merged image). In areas with actin accumulation, actin and activated rho colocalized (*insets*). Cytoplasmic-activated rho was also present away from the developing actin ring (top of field). *Bars* = 20 μm in low-magnification images and 7 μm in insets. (*B*) Activated rho is absent at the wound edge 8 minutes after wounding. Only small amounts of activated rho (red in merged image) remained at the wound edge by 8 minutes after wounding. The activated rho that was present did not colocalize with the actin ring (green in merged image). Damaged cells within the wound stained strongly (*) but nonspecifically. Controls using an irrelevant GST fusion protein in place of the GST-rhotekin rho binding domain fusion protein were negative under these imaging conditions. *Bars* = 20 μm in low-magnification images and 7 μm in insets.

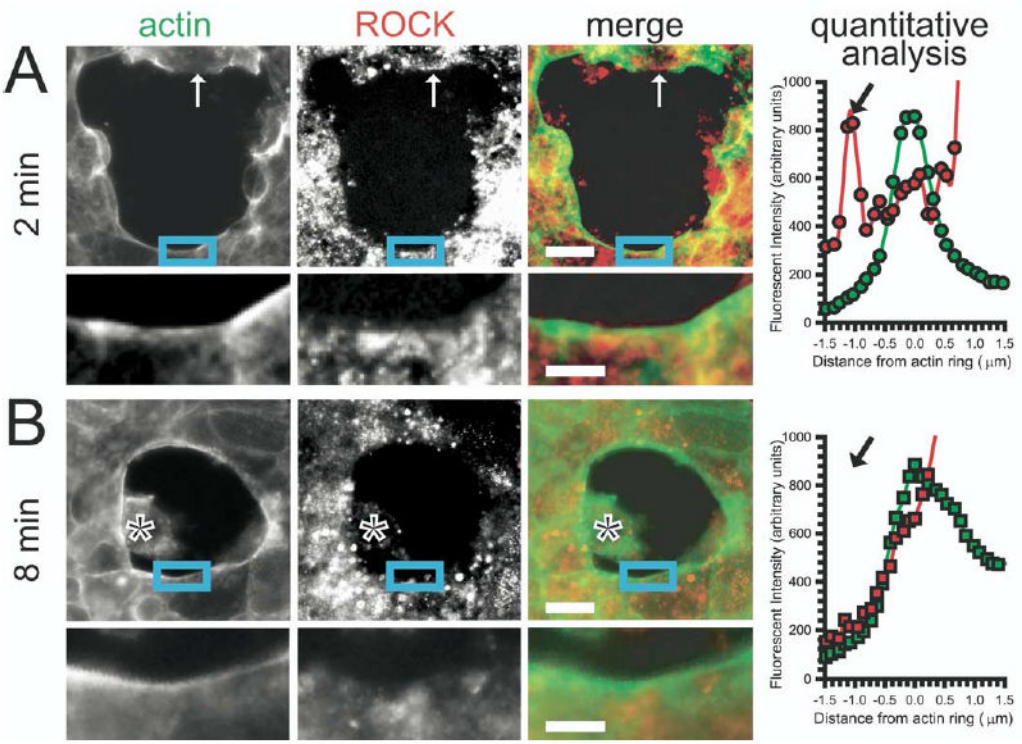

Figure 3.

(*A*) ROCK is present at the wound edge 2 minutes after wounding. Within 2 minutes after wounding, ROCK (*red* in merged image) was present in a discontinuous punctate pattern at the wound edge, both in association with (*insets*) and separate from (*arrows*) actin (*green* in merged image). ROCK was also detected in punctate cytoplasmic foci throughout the monolayer in cells remote from and bordering the wound. *Bars* = 20 μm in low-magnification images and 7 μm in insets. Quantitative analysis of ROCK and actin intensity was performed serially over the entire wound edge. To allow comparison of multiple areas, the location of the developing actin ring was set as zero with negative values closer to the center of the wound and positive values further away from the center of the wound. ROCK (*red*) and actin (*green*) intensity values are shown. A peak of ROCK is present just ahead of the developing actin ring (*black arrow*). ROCK then increases further away from the peak of actin, indicating detection of cytosolic ROCK not associated with the wound edge. (*B*) ROCK is lost from the wound edge by 8 minutes after wounding. Unlike early time points, ROCK (*red* in merged image) accumulation at the wound edge was not apparent by 8 minutes after wounding despite continued punctate cytoplasmic staining. The actin ring (*green* in merged image) is clearly visible. *Bars* = 20 μm in low-magnification images and 7 μm in insets. Quantitative analysis of ROCK and actin intensity was performed as previously described. ROCK (*red*) and actin (*green*) intensity values are shown. The peak of actin at 8 minutes is broader than at 2 minutes, indicating greater actin accumulation at this later time. Unlike earlier time points, no peak of ROCK is detected ahead of the actin ring (*black arrow*, compare with *A*). Like the earlier time point, cytosolic ROCK is detected behind the actin peak.

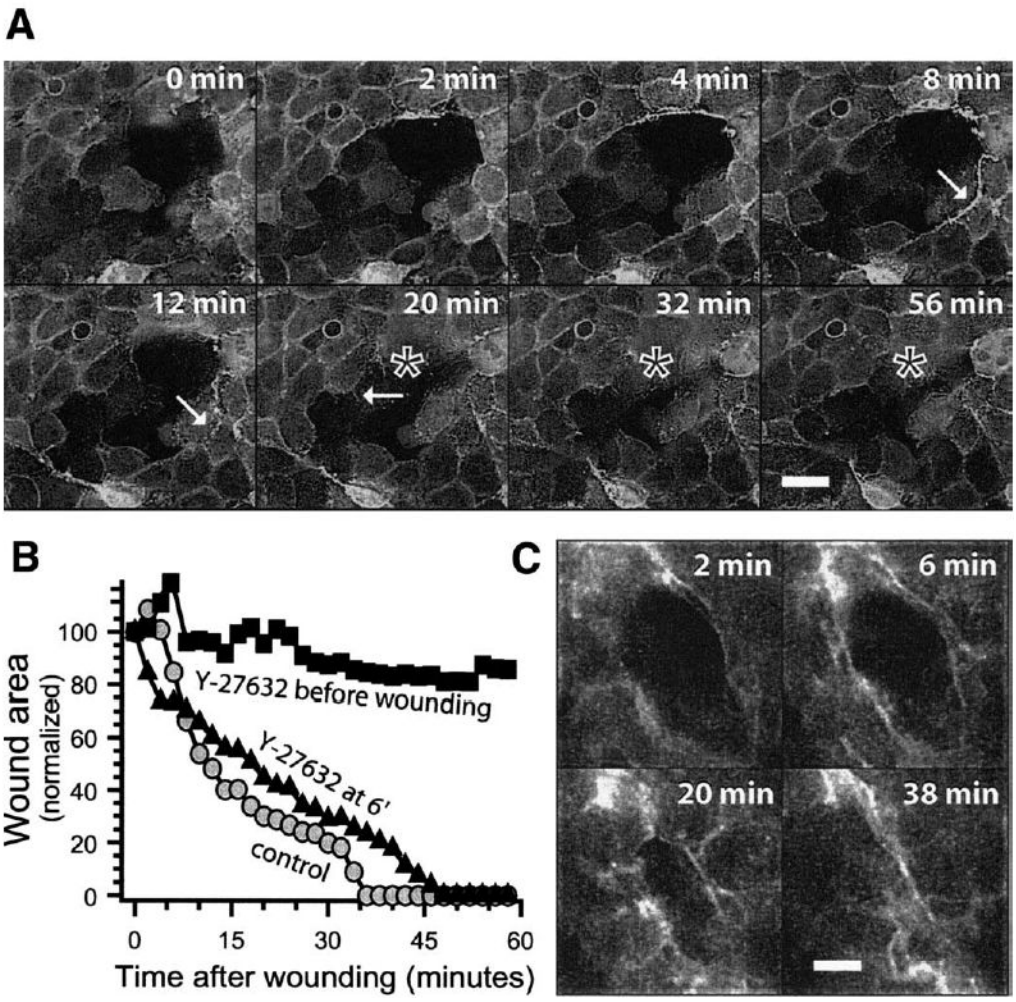

Figure 4.

(*A*) Wound closure is disrupted by ROCK inhibition (also see Movie 2; see supplemental material online at www.gastrojournal.org). Closure of an oligocellular wound in the presence of Y-27632, a ROCK inhibitor, added before wounding was studied as in Figure 1. Foci of actin polymerization appeared early in regions along the wound edge (8 minutes, *arrow*), similar to that seen in untreated wounds, but were unstable and a complete ring did not form (12 minutes, *arrow*). Unlike untreated wounds, cells surrounding the wound did not exhibit any meaningful contraction. Residual EGFP fluorescence-containing dead cells retained within the wound are apparent at early and late time points (*, compare with Figure 1*A*). Wound edges did not round, and no significant wound closure occurred. Focal filopodial extensions formed (20 minutes, *arrow*) but were transient and did not contribute to wound closure. *Bar* = 20 μm. (*B*) Quantitative analysis of wound closure when ROCK is inhibited before or after ring assembly. Wounds treated with Y-27632 before wounding did not show any meaningful wound closure (*black squares;* control wound data are included for comparison, *gray circles*). In contrast, when Y-27632 was added after actin ring assembly, wound closure proceeded normally (*black triangles* and *C*). (*C*) ROCK inhibition after ring assembly does not disrupt wound closure. Wounds treated with Y-27632 after ring assembly (ie, 6 minutes after wounding) followed a similar pattern and time course to control wounds. *Bar* = 20 μm.

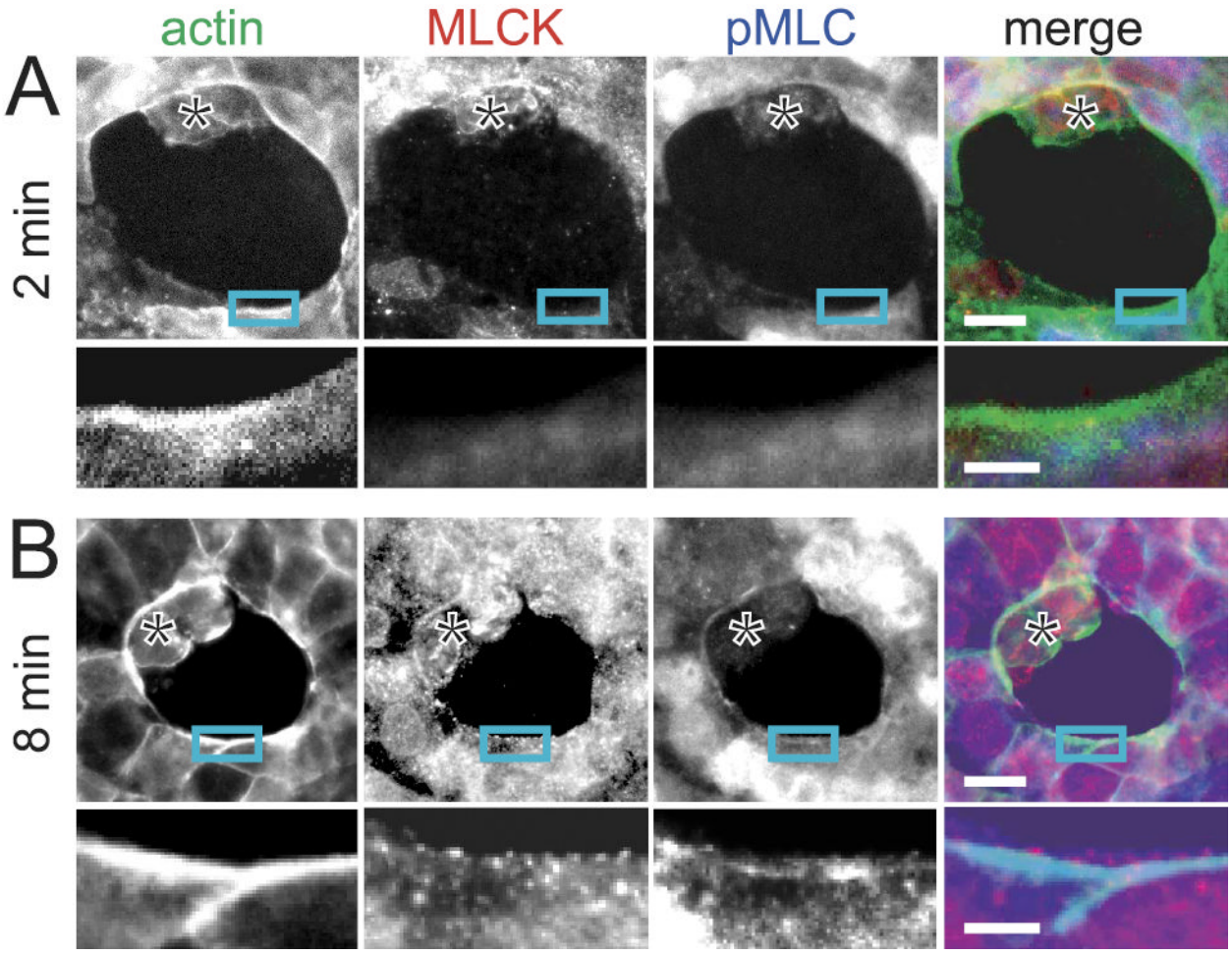

Figure 5.

(*A*) MLCK recruitment and MLC phosphorylation are minimal 2 minutes after wounding. MLCK (*red* in merged image) was only focally present at the wound edge 2 minutes after wounding, and these foci were always at sites of actin recruitment (*green* in merged image). MLC phosphorylation (pMLC; *blue* in merged image) was minimal at these early time points. Dead/damaged cells within the wound stain nonspecifically (*). *Bars* = 20 μm in low-magnification images and 7 μm in insets. (*B*) MLCK recruitment to and MLC phosphorylation at the wound edge coincide with the initiation of contraction. By 8 minutes after wounding, a punctate array of MLCK (*red* in merged image) was prominent at the wound edge. This MLCK recruitment was accompanied by phosphorylation of MLC (pMLC; *blue* in merged image). *Insets* reveal increased staining of MLCK and pMLC at the wound edge in areas of actin accumulation (*green* in merged image) 8 minutes after wounding. As at 2 minutes, nonspecific staining of dead cells within the wound is evident (*). *Bars* = 20 μm in low-magnification images and 7 μm in insets.

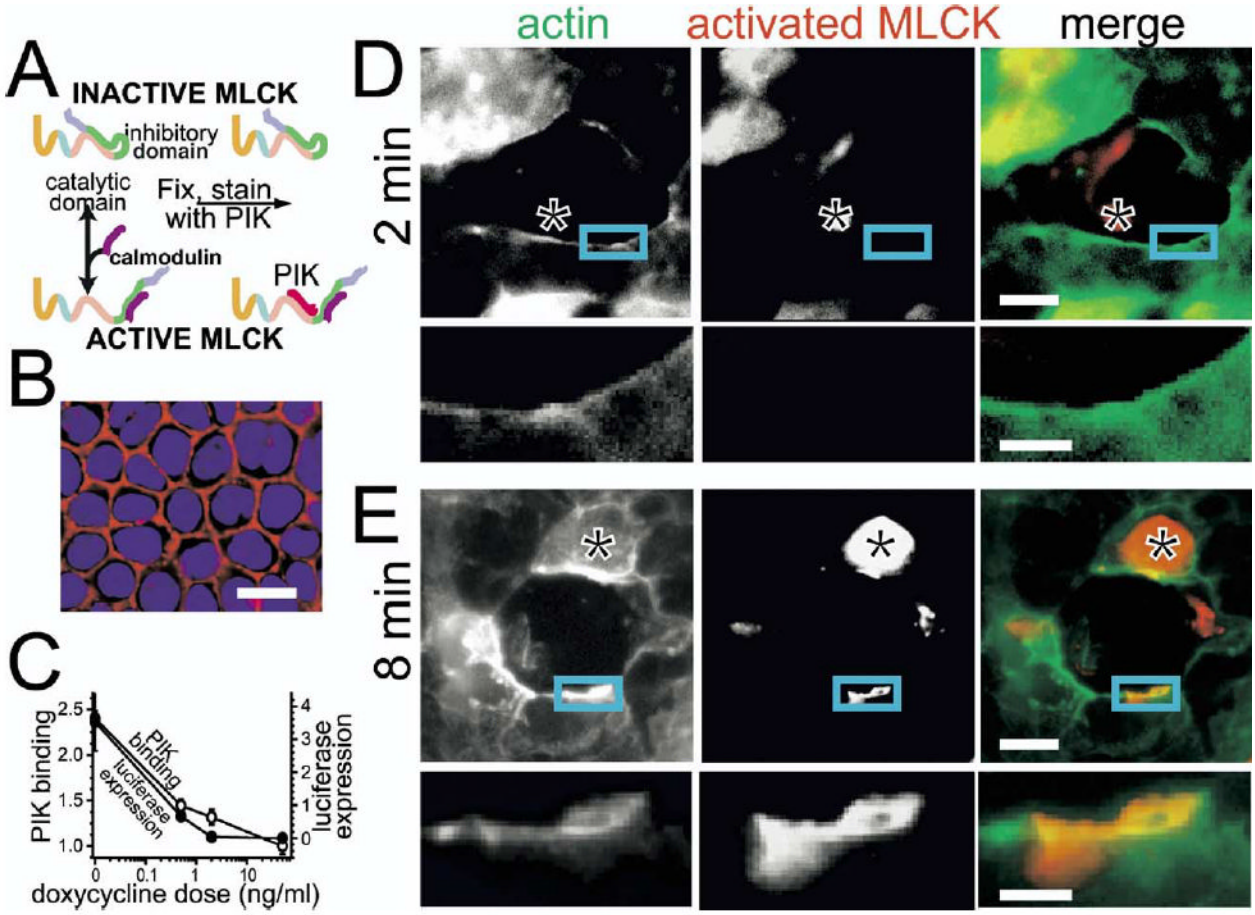

Figure 6.

(*A*) Model of PIK binding to active MLCK. This model of PIK binding to MLCK suggests that PIK can only bind to MLCK when it is in the active conformation. Thus, when MLCK is in the inactive conformation, PIK cannot bind and is washed away before detection with a secondary reagent. This property allows its use as a probe for activated MLCK. (*B*) PIK labels the perijunctional actomyosin ring. In steady-state monolayers, PIK binding is concentrated at intercellular junctions, a site of enhanced MLCK localization and MLC phosphorylation. Biotinylated PIK (*red*) and cell nuclei (*blue*) are shown. *Bar* = 20 μm. (*C*) PIK binds to activated MLCK. Caco-2 cells expressing the catalytic subunit of MLCK and firefly luciferase, both under the control of a tet-off expression system, were cultured in indicated doses of doxycycline. The cells were fixed and stained with biotinylated PIK and fluorescent streptavidin. Quantitative analysis of PIK binding showed that this correlated strongly with gene expression (luciferase, $r^2 = 0.98$), consistent with the model presented in *A*. (*D*) Activated MLCK is not present at the wound edge 2 minutes after wounding. Activated MLCK, as labeled with biotinylated PIK (*red* in merged image), was not present at early time points after wounding, when actin (*green* in merged image) ring assembly was incomplete. Exposures are matched between these images and *E*. Perijunctional staining (see *B*) is not visible because it was far less intense than staining at the wound edge (see *E*). Some nonspecific staining of debris within the wound (*) is apparent. *Bars* = 20 μm in low-magnification images and 7 μm in insets. (*E*) Activated MLCK is present at the wound edge at 8 minutes after wounding. Activated MLCK (*red* in merged image) was focally present at the wound edge 8 minutes after wounding and colocalized with actin (*green* in merged image). The bright nuclear staining (*) was occasionally seen regardless of wound status and likely reflects nonspecific interactions

between DNA and the highly charged PIK peptide. *Bars* = 20 μm in low-magnification images and 7 μm in insets.

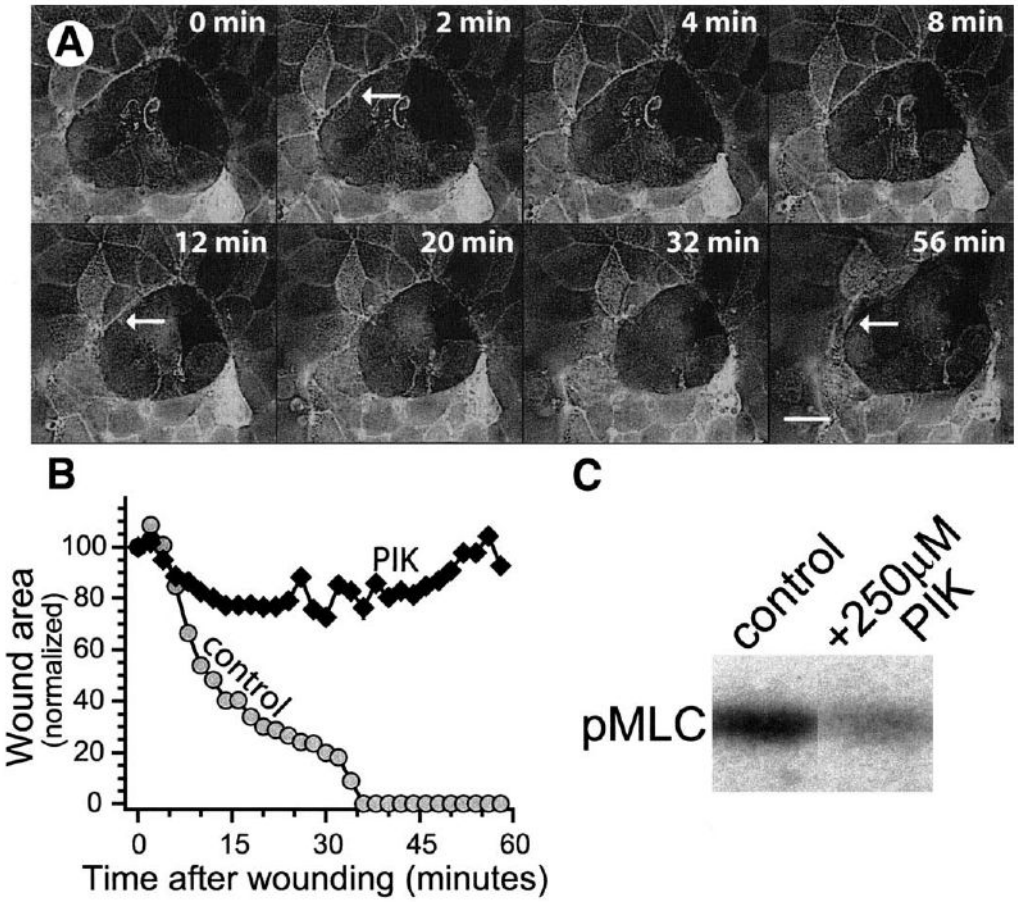

Figure 7.

(*A*) Wound healing is delayed and ultimately inhibited by PIK, a specific MLCK inhibitor, in oligocellular cell wounds (also see Movie 3; see supplemental material online at www.gastrojournal.org). MLCK inhibition by PIK did not prevent actin ring assembly (*arrows* at 2 and 12 minutes) or early wound edge rounding. However, the ring then began to fragment (*arrow* at 56 minutes). The wound enlarged and appeared to spring back to the original area. Note faint residual cell debris within the wound. *Bar* = 20 μm. (*B*) Wound area diminishes briefly but then expands when MLCK is inhibited. In monolayers treated with PIK, wound area initially decreased similar to that of control wounds, but by 8 minutes the rates of closure diverge. With MLCK inhibition wound area decreased only slightly after 8 minutes and ultimately expanded to its original area. (*C*) PIK effectively inhibits MLCK. In vitro kinase reactions show that 250 μmol/L PIK inhibits >70% of MLC phosphorylation.

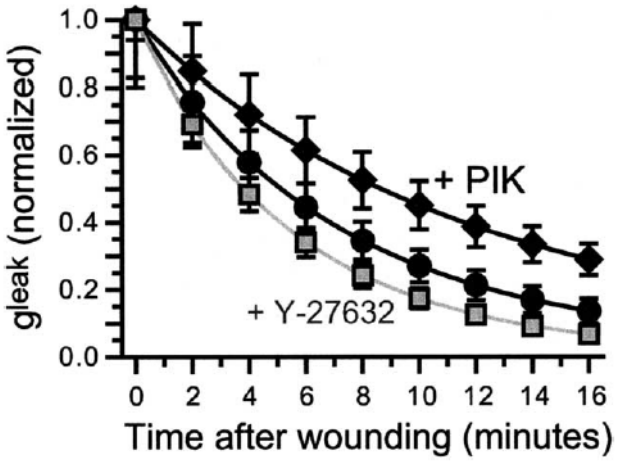

Figure 8.

MLCK inhibition delays but does not prevent restoration of barrier function after single-cell wounds. In control cells, the magnitude of the conductance leak (g^{leak}) decreased exponentially over time after wounding. Between 2 and 8 minutes after wounding, g^{leak} decreased by 53% (from 0.41 ± 0.07 to 0.19 ± 0.03 microSiemens; n = 7; $P < .01$) in control experiments. A single-exponential fit revealed a time constant of 8.67 ± 1.40 min (n = 7) and was used to estimate g^{leak} during the 2-minute interval between wounding and the beginning of measurements. With increasing time after wounding, g^{leak} approached zero asymptotically and barrier function of the epithelium was similar to that before wounding. Monolayers incubated with PIK showed delayed repair kinetics. Between 2 and 8 minutes after wounding, g^{leak} decreased by only 36% (from 0.52 ± 0.09 to 0.32 ± 0.05 microSiemens; n = 9; $P < .05$ relative to control wounds). The time constant was 15.14 ± 2.21 minutes (n = 9; $P < .05$ relative to control wounds). Even 16 minutes after wounding, g^{leak} in PIK-treated wounds remained elevated relative to control wounds (0.18 ± 0.03 microSiemens with PIK vs 0.07 ± 0.02 microSiemens; n = 9; $P < .01$). Representative data using the ROCK inhibitor Y-27632 are provided for reference (n = 8; $P > .05$ vs control).[9]

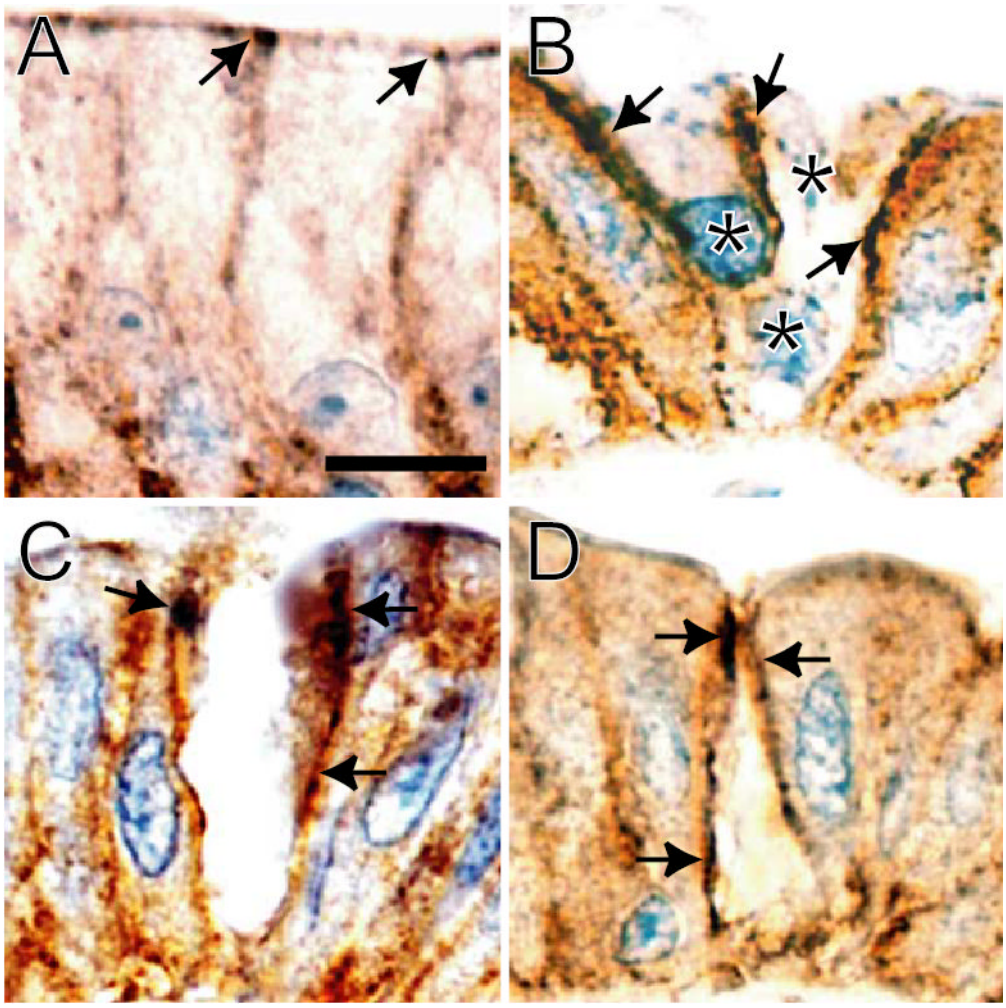

Figure 9.

MLC phosphorylation occurs at the edge of human oligocellular wounds. Colonic biopsy specimens from patients with active inflammatory bowel disease (both Crohn's disease and ulcerative colitis) were immunohistochemically stained for phosphorylated MLC (*brown*). A light hematoxylin counterstain (*blue*) was then applied. (*A*) Nonwounded mucosa. As we have noted previously,[26] MLC phosphorylation is enhanced at the site of the tight junction (*arrows*) in normal mucosa. No staining was detected when an irrelevant primary antiserum was used. In oligocellular wounds (*B–D*), MLC phosphorylation is markedly enhanced along the lateral edges of the wound (*arrows*). *Bar* = 5 μm. (*B*) As in the Caco-2 model, dead/damaged cells are retained within some wounds (*). Although from separate biopsy specimens in different patients, *B–D* have been arranged in a sequence consistent with progressive wound closure. Three nuclei of damaged or dead cells are apparent within the wound shown in *B*. (*C*) Nuclei of dead cells are not apparent, and MLC phosphorylation has extended over nearly the full height of the wound. (*D*) Ring contraction continues with sealing of the apical portion of the wound.

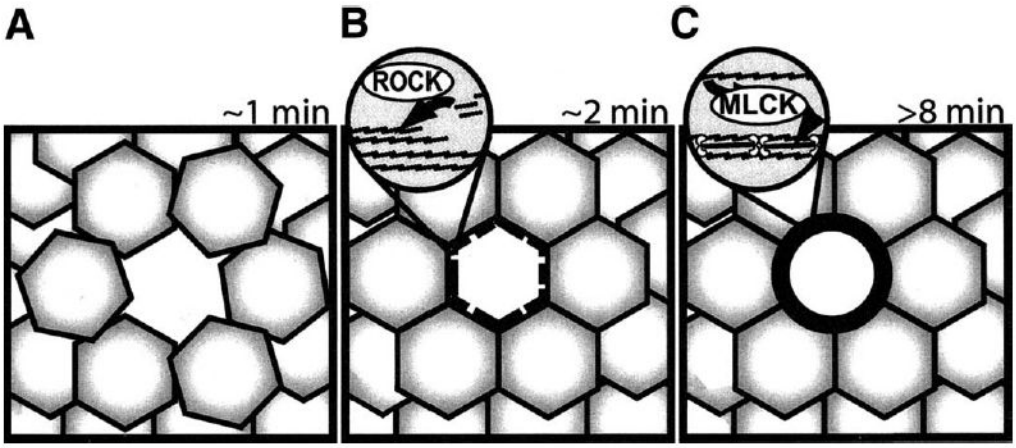

Figure 10.

Model describing the roles of ROCK and MLCK during epithelial purse-string wound closure. (*A*) Schematic of initial wound within a previously intact epithelial sheet. A continuous multicellular actin ring is not present at the wound edge, and the profile of the wound is irregular. (*B*) The actin ring assembly phase, where ROCK, activated by rho, directs the recruitment and assembly of actin filaments to form a continuous ring at the wound edge. However, wound contraction has not been initiated and the wound profile remains irregular. (*C*) The contraction phase, where MLCK-mediated MLC phosphorylation triggers actomyosin contraction, providing the driving force for epithelial purse-string wound closure and rounding the wound edges.